Northumbria Research Link

This version was downloaded from Northumbria Research Link: http://nrl.northumbria.ac.uk/id/eprint/38319/

Northumbria
University
NEWCASTLE

University**Library**

Hybrid thermal storage using coil-encapsulated phase change materials

C.P. Underwood[1], T. Shepherd[2], S.J. Bull[3], S. Joyce[3]

1.   Faculty of Engineering and Environment, Northumbria University, Newcastle upon Tyne NE1 8ST, UK
2.   Community Energy Solutions, Leeds LS2 7JU
3.   School of Chemical Engineering and Advanced Materials, Newcastle University, Newcastle upon Tyne NE1 7RU

HIGHLIGHTS

- Hybrid thermal storage using phase change material (PCM) in coils is evaluated.
- A new method for relating the enthalpy and temperature of the PCM is proposed.
- Thermal store design parameters are extracted from experimental data.
- Simulations carried out for grid-stress mitigation using a heat pump/store combination.
- The hybrid store shows improved comfort during grid-stress periods in winter.

ABSTRACT

Compact thermal storage using a hybrid phase change material (PCM) store for domestic heating applications is investigated in this work. The primary focus is to support heating and hot water demand during the electrical grid-stress period which occurs during 16:00h – 20:00h on winter weekdays. Previous research has focused on PCM encapsulated in spheres or straight tubes whereas this work considers PCM encapsulated in pipe coils surrounded by water in an otherwise conventional hot water storage tank. Two alternative samples of salt hydrate are evaluated experimentally and the results are used to extract model parameters including the mean water-PCM thermal transmittance value. A new model is proposed for relating the enthalpy and temperature of the PCM during melting and solidification. A compact hybrid store design is proposed and a detailed thermal model of the hybrid store with an air-source heat pump is constructed and applied to an example house. Seasonal energy results compared with a conventional water tank are broadly similar but the hybrid store offers better comfort tracking during grid stress periods – average house temperatures falling below 19°C for 22.7% of the time with a conventional store but only 5.8% of the time using the hybrid store.

List of symbols

A	Area (m^2)
ACR	Air change rate (h^{-1})
AU	Area-integrated thermal transmittance (kWK^{-1})
C	Thermal capacity (kJK^{-1}, Jm^{-2}K^{-1})
c	Specific heat capacity (kJkg^{-1}K^{-1})
$\bar{c}$	Mean specific heat capacity (kJkg^{-1}K^{-1})
E	Energy (kWh)
F	Fitting parameter for PCM h-T model (-)
f	Resistance rationing factor (-)
FR	Radiant emission fraction (-)
g	Capacitance rationing factor (-)
$Goal$	Optimization objective function goal (K)
h	Enthalpy (kJkg^{-1})
I	Solar irradiance (Whm^{-2})
K	Tank ambient heat loss coefficient (WL^{-1}K^{-1})
M	Static mass (kg)
m	Mass flow rate (kgs^{-1})
N	Day number (-)
n	Discretised model zone number (-)
$\mathbf{P}$	Optimisation algorithm parameter vector
$\mathbf{P^{min}}$	Minimum parameter vector values
$\mathbf{P^{max}}$	Maximum parameter vector values
Q	Heat transfer (W, kW)
$RMSE$	Root-mean-square error (K)
R	Fabric thermal resistance (m^{2}KW^{-1})
$SCoP$	Seasonal coefficient of performance (-)
SPF	Seasonal performance factor (-)
T	Temperature (^{o}C)
t	Time (s)
U	Fabric thermal transmittance value (Wm^{-2}K^{-1})
V	Volume (m^3)
W	Power (W)
x	Axial distance (m)
α	Surface-solar azimuth (degree)
β	Surface angle of tilt (degree)
Δt	Time step size (s)
ρ	Density (kgm^{-1})
ϕ	Site latitude (degree)
τ	Window glass transmissivity (-)
θ	Time constant (s)

List of subscripts

a	Air
ai	Air, internal
al	Ambient environment
ao	Air, external
aux	Auxillary
boost	Boost heater
buffer	Buffer storage
cas	Casual (heat gain)
ch	Charge phase
co	Condenser
cwf	Cold water feed
des	At design conditions
dhw	Domestic hot water
dis	Discharge phase
ev	Evaporator
F	At (nominal) fusion point
g	Ground
h	Heating
hor	Horizontal
hp	Heat pump
i	Inlet, infiltration
max	Maximum
o	Outlet
past	Pasteurising heater
pcm	PCM zone
pinch	Pinch point (heat exch.)
pri	Primary (heating)
v	Ventilation
w	Water zone
wi	Water inlet zone
wii	Inlet to water inlet zone
wo	Water outlet zone
wp	Water/PCM boundary
0	Initial state

Abbreviations

PCM	Phase change material
S32	PCM sample 1 (32°C)
S46	PCM sample 2 (46°C)

1. Introduction

Heat pumps are embarking on a period of rapid growth for domestic heating in order to reduce carbon emission as well as to help to diversify the heating energy mix. In the UK for example, a current dependence on gas heating boilers for approximately 80% of housing is expected to give way to a significant take-up of both air- and ground-source heat pumps and their hybrids in the coming years [1]. Continuing progress on the introduction of cleaner and more sustainable forms of electricity generation will accelerate this trend.

A particular challenge with increased heat pump use is the question of electricity grid capacity and the need for its reinforcement. Peak demand for electricity tends to occur on winter weekdays starting at about 16:00h. Using data from [2], Fig. 1 shows the daily weekday demand profile for four randomly-selected weekdays in November 2015 through February 2016 in the UK. A consistent period of electricity demand growth starting at 16:00h and running through until about 20:00h is evident. In this paper, this will be referred to as the 'grid-stress' period.
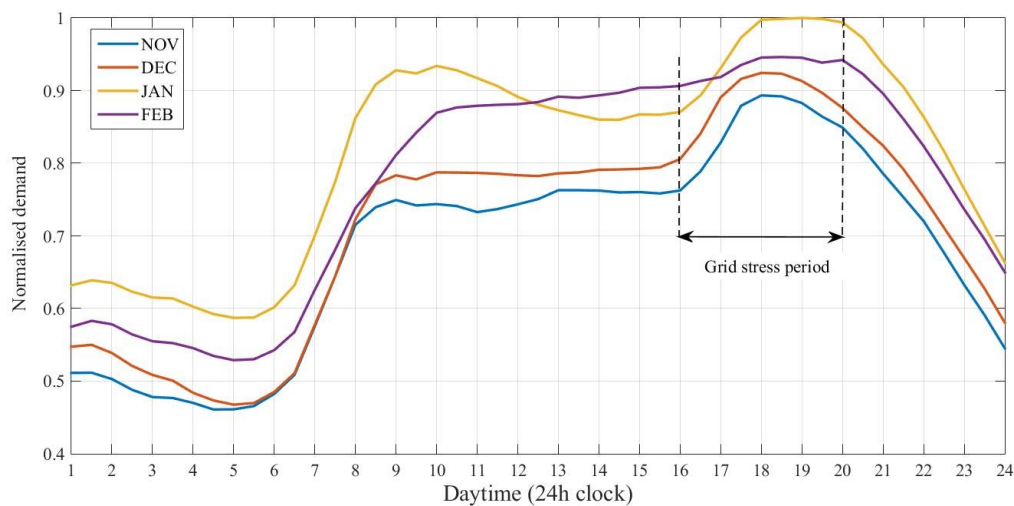
Fig. 1. Normalised UK power demands (random weekdays Nov 2015 – Feb 2016)

The growth part of the grid-stress period unfortunately coincides with the typical day time switch-on point for most domestic heating systems in housing as workers begin to return home for the evening. Therefore, growth in electric heat pumps for domestic space heating will severely exacerbate the grid-stress problem. Measures are therefore needed to head this problem off consisting either of electrical grid reinforcement (expensive) or through the introduction of local energy storage enabling the heat pump to start at a time outside the grid-stress period such that the energy storage system can contribute to satisfactory space heating continuity through this period whilst the heat pump remains idle or at very light load. In practice, it is likely that a combination of these measures will be needed as energy infrastructures move forward in this way. For electric heat pumps, the energy storage option can be considered on the thermal (heating system) side of the system or, conceivably, on the electrical connection side of the system in the form of batteries. Recent developments in high energy density phase change materials (PCMs) make the former method particularly promising. In this paper, the development of a compact thermal storage system based on PCM for the specific purpose of grid-stress mitigation when heat pumps are used is considered.

The aim of the research reported in this paper is to develop and evaluate a proposed design for a compact thermal storage system using phase change material suitable for coupling to a conventional domestic heat pump for hot water space heating and domestic hot water heating. A particular focus of the research is the offset of heating demands that occur through the grid-stress period. A particular feature of the work is that the encapsulation of PCM in coils is considered – something that has not previously been reported in the literature.

The objectives are as follows:

- To develop a test facility for the purpose of measuring the response of coil-encapsulated phase change material (PCM) in a water storage tank.
- To develop a mathematical model of a hybrid PCM/water thermal store parameterised from results obtained from the test facility.
- To propose a design framework for a hybrid PCM/water thermal store for use in a typical modern (well-insulated) house.
- To extend the mathematical model into a full domestic heating simulation and evaluate the performance of the integrated system with particular reference to the grid-stress period.
- To evaluate seasonal energy, heat pump performance and thermal comfort of the integrated system benchmarked against an alternative use of a conventional water tank thermal store.

2. Previous Work

Material developments, encapsulation and applications to thermal storage systems of PCMs have received substantial attention in the past 25 years and, particularly, in the past 10 as evidenced by the large number of review-type papers on the subject [3-9]. One of the earliest and one of the most comprehensive of the research reviews includes extensive listings of typical material properties including single salt hydrates, salt blends (eutectics) and organic compounds [3]. Agyenim *et al*. [4] also present details of a range of PCM properties showing that, for many materials, thermal conductivities are generally low but generally higher in the solid phase than in the liquid phase. This has implications for heat transfer rates during both charging (melting) and discharging (solidification). They also review heat transfer enhancement and containment methods. Further examples can be found in the review of de Cunha and Eames [5] concluding that salt hydrates and organic compounds form the most promising materials for applications below 100ºC. A number of reviews have been presented on the application of PCMs in storage systems forming parts of domestic and small scale heating systems including domestic hot water [6,7] and heat pumps [8,9].

Rastogi *et al*. developed methods for ranking PCMs for the purpose of selection for specific applications [10]. The methods were limited to low temperature materials transitioning at 17-25ºC (i.e. mainly for use as building structure enhancements) although there is no reason why the methods presented could not be applied to other applications.

Quantitative research into PCMs and their applications have involved experimental work [11-16] and numerical modelling [17-22]. Choi and Kim investigated heat transfer using a salt hydrate (magnesium chloride hexahydrate) surrounding plane and externally-finned tube options carrying compressed air as the heat transfer medium [11]. They measured *U*-values ranging from 160-200Wm^{-2}K^{-1} in the conductive region for the plane tube option with ratios of 1.1 – 2.1 for finned tubes, depending on fin spacing. They found convective contributions

to be significant when the material was fully melted. Agyenim and Hewitt carried out an experimental investigation of paraffin wax PCM in a horizontal cylinder encapsulation with an embedded finned tube through which heat transfer fluid in the range 62-77°C is delivered [12]. They observed different U-values during the charge and discharge phases of 16-23.5Wm^{-2}K^{-1} in the charge phase and 15-19.5Wm^{-2}K^{-1} during discharge – much lower than Choi and Kim's work with salt hydrate [11] though the experimental set-ups were quite different. The higher U-values in the charge (melting) phase are to be expected in part due to the material having higher conductivity in the solid phase (as shown, for example, in [4]). Frazzica et al. carried out an experimental evaluation of both paraffin and salt hydrate PCMs with nominal melting points of 65°C and 58°C respectively [13]. Both samples are contained in polypropylene capsules, alternately immersed in a tank of water. The results show an increase in hot water delivery of about 10% using the salt hydrate though small test volumes of PCM were used. Twice the quantity of the paraffin-based sample was needed for the same heat storage due to lower material density. Murray and Groulx did an experimental investigation of the charging and discharging transient behaviour of dodecanoic acid (which melts at 42.5°C) for solar domestic hot water applications [14]. Their experimental facility consisted of a vertical vessel containing PCM with two externally-finned tubes passing through the PCM, one of which circulating hot water (for melting) and the other cold water (for solidification). They also found that natural convection played a significant part in heat transfer during charging (melting) but not so during discharging. Porteiro et al. investigated three alternative salt hydrate PCMs in three alternative encapsulations (two involving polymer cylinders and a third involving a micro-encapsulation method) tested in a 100L water tank [15]. The transitioning temperatures of the three samples varied in the range 50-61°C. The sample masses varied in the range 13.8kg – 31kg. The microencapsulation method was found to give shorter solidification times than the cylindrical encapsulations. Zauner et al. carried out an experimental evaluation of a hybrid store consisting of high density polyethylene PCM inside the tubes of a shell and tube heat exchanger with thermal oil as the (shell-side) heat transfer fluid [16]. This is a high temperature application (140-160°C) for district heating applications.

In numerical work, Kelly et al. investigated off-peak heating using a heat pump coupled to a thermal store [17]. For the case study house that they considered, they concluded that a 1000L water tank would be needed for complete load shifting or a 500L PCM-enhanced thermal store (with a void fraction of 50%). Khan et al. modelled the use of paraffin PCM in the void space of a shell and tube heat exchanger with various tube pass, material and exterior fin details [18]. The choice of material for tube and fin construction was found to be influential. Campos-Celador et al. presented details of the design of a finned-plate hybrid thermal storage system using an organic PCM and compared the design with a 500L conventional water tank [19]. They concluded that the hybrid design would need to be approximately half of the volume of the conventional water tank storage system to give the same heat storage. Najafian et al. considered the impact of putting different quantities of PCM (sodium acetate trihydrate) into a 270L domestic hot water storage tank [20]. Various simulations are used to find the best balance of PCM to water concluding that 32-35kg of PCM would provide sufficient storage for one day's domestic hot water draw-off.

Some of the recent work has focused on using additives to enhance the inherently low thermal conductivity of many established PCMs so that heat transfer powers of hybrid PCM storage systems can be increased. For example, Nabavitabatabavi et al. did a numerical study of pure PCM and nano-particle-enhanced PCM occupying vertical plain tubes inserted in a water tank [21]. They concluded that nano-particle enhancement considerably reduces the solidification times of the PCM and Pincemin et al. investigated graphite additives to PCM as a means of

increasing the effective thermal conductivity in higher temperature thermal storage applications [22].

In summary, considerable research has been reported on PCM applications for enhanced and hybrid thermal storage systems. Most of the focus to date has been in the use of PCM occupying the void space through which heat transfer fluid in plain straight tubes or finned tubes passes, or on PCM encapsulated in straight tubes with the heat transfer fluid flowing over the outside. In the use of PCM in small (e.g. domestic) applications, the focus has been mainly on solar domestic hot water storage and heat pumps linked to thermal storage for use in off-peak heating. In the work reported here, two new applications are considered – PCM encapsulated in helical coils for use in short term thermal storage to mitigate the impact on electrical grid stress. Furthermore, a new perspective on modelling these systems is proposed.

3. Determination of Heat Transfer Coefficients

Two alternative samples of salt hydrate PCM were dosed into the internal primary heating coils of an otherwise conventional hot water storage tank. The tank contained two concentric coils (the outer one visible in Fig. 2 (left)).

3.1. Modelling

It was possible to dose 19 litres of each sample, in turn, into the two internal coils. The nominal overall tank capacity was 305 litres. The two samples of salt hydrate had nominal melting temperatures of 32ºC and 46ºC respectively. Charge and discharge tests were carried out on the first sample after which it was melted, flushed out of the coils, and then replaced with the second sample and further tests carried out. The samples were prepared in a 20L electric melting tank and pumped into the coils using a progressive-cavity pump.

The charge and discharge test results may be used to parameterise a mathematical model of the resulting water/PCM hybrid storage tank. Reference is made to the simplified zoning layout illustrated in Fig. 1 (right). Assuming perfect lateral mixing (i.e. variations considered along the x flow path only) an energy balance at the tank inlet zone can be written as Eq. (1).
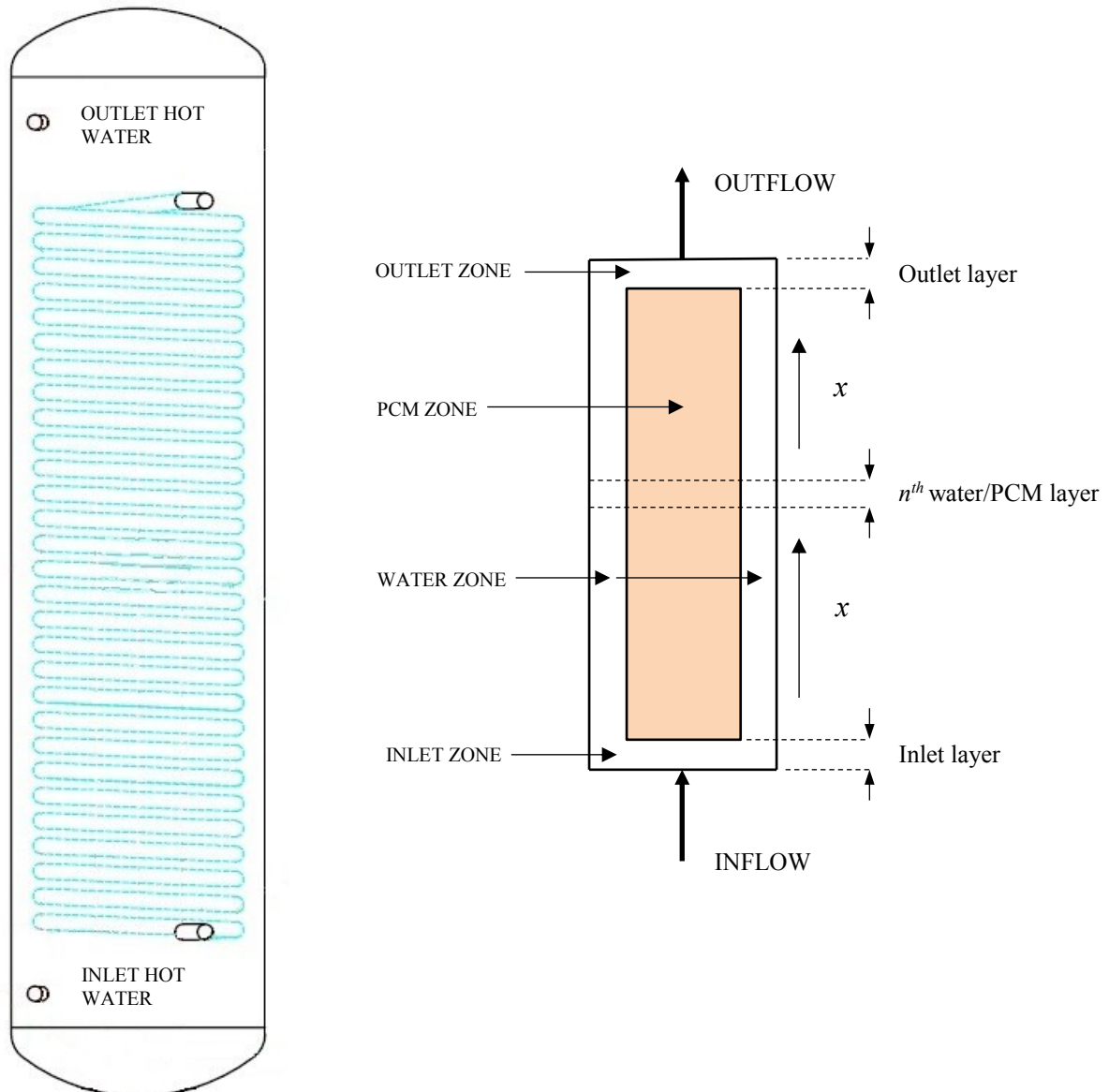
$$C_{wi} \frac{\partial T_w}{\partial t} = m_w c_w \frac{\partial T_w}{\partial x} - A U_{al\text{-}i}\left(T_w - T_a\right) \tag{1}$$

In the water/PCM zone, the energy balances in the water and PCM sub-zones are respectively given by Eq. (2) and Eq. (3).

$$C_{wp} \frac{\partial T_w}{\partial t} = m_w c_w \frac{\partial T_w}{\partial x} - A U_{wp}\left(T_w - T_{pcm}\right) - A U_{al\text{-}wp}\left(T_w - T_a\right) \tag{2}$$

$$M_{pcm} \frac{\partial h_{pcm}}{\partial t} = A U_{wp}\left(T_w - T_{pcm}\right) \tag{3}$$

in which $T_{pcm} = f(h_{pcm})$, to be dealt with in Section 3.2.

Fig. 2. Thermal storage tank (left: actual, right: simplified zoning)

Finally, the outlet water zone energy balance is obtained from Eq. (4).

$$C_{wo} \frac{\partial T_w}{\partial t} = m_w c_w \frac{\partial T_w}{\partial x} - A U_{al\text{-}o} (T_w - T_a) \tag{4}$$

The equations were discretised using a backward-in-time scheme. The rationale for this is that it provided flexibility regarding the choice of calculation time step which was largely governed by the sampling interval used in measurements of the hybrid thermal store. A further justification is that backward-in-time gives unconditional stability whilst forward-in-time would require careful selection of calculation time step to give stable outputs. Discretisation of equations (1-4) resulted in equations (5-8) with respect to the nth layer in the water/PCM zone. Since the water volumes in both the inlet and outlet zones of the tank are low, a single zoning layer was used for these two zones.

$$T_{\text{wi}(t)} = \frac{C_{\text{wi}}T_{\text{wi}(t-\Delta t)} + \Delta t\left(m_{\text{w}}c_{\text{w}}T_{\text{wii}(t)} + A\,U_{\text{al-i}}T_{\text{a}}\right)}{C_{\text{wi}} + \Delta t\left(m_{\text{w}}c_{\text{w}} + A\,U_{\text{al-i}}\right)} \tag{5}$$

$$T_{\text{w}(n,t)} = \frac{C_{\text{w}(n)}T_{\text{w}(n,t-\Delta t)} + \Delta t\left(m_{\text{w}}c_{\text{w}}T_{\text{w}(n-1,t)} + A\,U_{\text{wp}(n)}T_{\text{pcm}(n,t)} + A\,U_{\text{al-wp}(n)}T_{\text{a}}\right)}{C_{\text{w}(n)} + \Delta t\left(m_{\text{w}}c_{\text{w}} + A\,U_{\text{wp}(n)} + A\,U_{\text{al-wp}(n)}\right)} \tag{6}$$

$$h_{\text{pcm}(n,t)} = h_{\text{pcm}(n,t-\Delta t)} + \frac{\Delta t A\,U_{\text{wp}(n)}}{M_{\text{pcm}(n)}}\left(T_{\text{w}(n,t)} - T_{\text{pcm}(n,t)}\right) \tag{7}$$

$$T_{\text{wo}(t)} = \frac{C_{\text{wo}}T_{\text{wo}(t-\Delta t)} + \Delta t\left(m_{\text{w}}c_{\text{w}}T_{\text{w}(n_{\text{max}},t)} + A\,U_{\text{al-o}}T_{\text{a}}\right)}{C_{\text{wo}} + \Delta t\left(m_{\text{w}}c_{\text{w}} + A\,U_{\text{al-o}}\right)} \tag{8}$$

3.2. Enthalpy-temperature relationship

In theory, the PCM should melt and freeze at a constant temperature which implies an abrupt functional relationship between enthalpy and temperature. Experience however points to a more gradual transition between solid and liquid states particularly when additives have been included in order to, typically, increase the long term stability of the material or to reduce its corrosivity. Also, for a number of materials, the freezing point can be lower than the melting point due to super cooling effects. A smoother transition between solid and liquid states implies a region in which the material is partly solid and partly liquid – a so-called 'mushy' region as illustrated in Fig. 3. A smooth transition between extreme states in a relationship, $y = \text{f}(X)$, can conveniently be represented using a sigmoid function of the form: $y = K / (1 + \text{e}^{bX})$ in which K and b are constants. With the addition of sensible heating effects prior to, and after, phase transition, such a relationship for a PCM might be anticipated in Eq. (9).

$$h_{pcm(t)} = \bar{c}_{pcm}\left(T_{pcm(t)} - T_{pcm}(0)\right) + \frac{h_{pcm-F}}{1+\exp\left(F\left(T_{pcm-F} - T_{pcm(t)}\right)\right)} \tag{9}$$

in which h_{pcm-F} and T_{pcm-F} are the latent heat of fusion of the PCM and the nominal melting/freezing temperature respectively and $T_{pcm}(0)$ is an arbitrary thermodynamic reference temperature. This equation provides closure for equations (5)-(8).
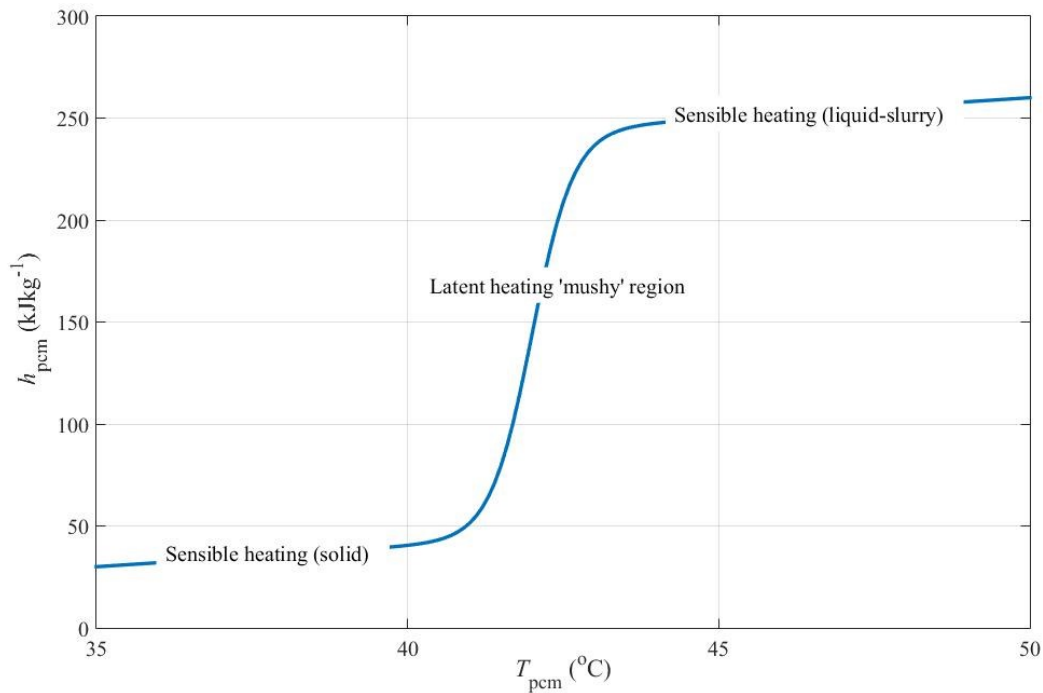
Fig. 3. Typical *h-T* relationship for a phase change material

3.3. Parameter extraction method

Experiments were conducted on two samples of salt-hydrate PCM. The samples were individually dosed into the internal coils of a conventional hot water tank and the coils were surrounded by system water. Samples of solid PCM blocks (Fig. 4(b)) were first melted in a melting tank and then pumped into the tank's coils using a positive-displacement pump (Fig. 4(c)). Each experiment consisted of contiguous charge and discharge periods. During the charge period, warm water from a ground-source heat pump (Fig. 4(a)) was circulated through the tank at a temperature approximately 5K higher than the nominal phase change temperature for the sample under test. The charge phase was deemed to have concluded as the temperature difference across the water connections to the tank approached zero. During the discharge phase, the heat pump was switched off and the tank water was circulated through a nearby system of hot water radiators in the laboratory.
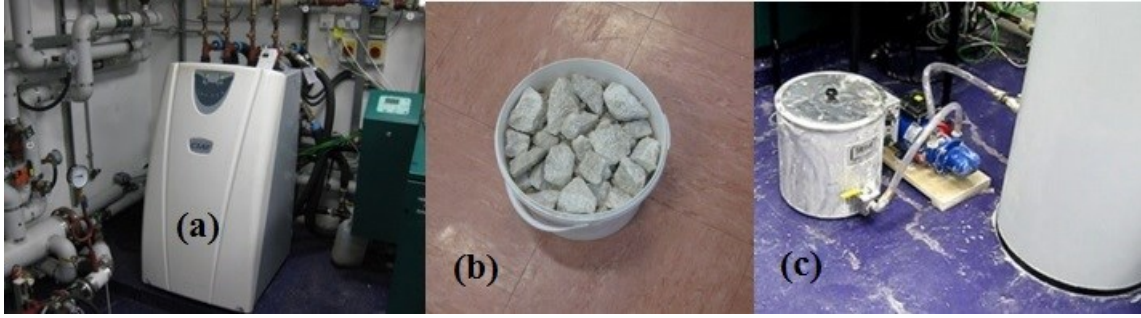
Fig. 4. (a) Heat pump; (b) Raw PCM sample; (c) Melter, dosing pump and tank

Again, discharge was deemed to have concluded as the temperature difference across the water connections to the tank were noted to have approached zero.

Equations (5)-(9) were coded into a Matlab function with an outer time loop and an inner spatial loop. At each time interval, the equations were stepped through in spatial sequence repeatedly until consecutive sets of spatial zone temperatures were all in agreement to within a small tolerance (0.05K) – i.e. Gauss-Seidel iteration. At this point, time is advanced by one time step and the inlet water temperature value is updated and the iteration repeats again. The parameters of interest were: $\mathbf{P} = [h_{\text{pcm-F}}, T_{\text{pcm-F}}, \bar{c}_{\text{pcm}}, \rho_{\text{pcm}}, F, AU_{\text{wp}}]$. Though the first four of these were available from information provided by the PCM suppliers [25], they were included so that they could be verified. The last two parameters are unknown.

Two experiments were carried out for each of the two PCM samples. The two samples had nominal transition temperatures of 32ºC and 46ºC labelled here for convenience as S32 and S46, respectively. Results of the first experiment for each sample were used to fit values to the parameter set described above. Results of the second experiment were used to test the resulting fitted model. The fitting and testing was carried out in two stages – the charge stage and the discharge stage. This would then reveal any differences in the mean AU_{wp} value (in particular). Parameter fitting was carried out using a constrained optimisation algorithm seeking to minimise the root-mean-square error, *RMSE*, between the transient model-predicted and measured tank outlet water temperatures (Eq. (10)).

$$\min_{\mathbf{P}} RMSE \quad \text{subject to:} \quad \begin{cases} RMSE \leq Goal \\ \mathbf{P} \geq \mathbf{P^{min}} \\ \mathbf{P} \leq \mathbf{P^{max}} \end{cases} \tag{10}$$

Temperature measurement was conducted using 'T' type thermocouples with an uncertainty of ±0.5K. The required *Goal* value was set below this value in order to seek an outcome that was within measurement uncertainty. The initial estimate of the first four values of **P** were set according to values given by the supplier of the PCM samples [25]. The search space for these values was restricted to ± 10% since it was not expected that results would stray too far from the supplier's values. However the range of results for both F and AU_{wp} was less certain and a wider range of values in $\mathbf{P^{min}}$, $\mathbf{P^{max}}$ was used (Table 1).

Table 1
Initial parameter estimates and assumed ranges

Sample	Parameters	h_{pcm-F} (kJkg^{-1})	T_{pcm-F} (°C)	$\bar{c}_{pcm}$ (kJkg^{-1}K^{-1})	ρ_{pcm} (kgm^{-3})	F (-)	AU_{wp} (kWK^{-1})
S32	**P(0)**	200	32	1.91	1460	1	0.25
	P^{min}	180	29	1.70	1300	0.25	0
	P^{max}	220	35	2.10	1600	3	0.50
S46	**P(0)**	210	46	2.41	1587	1	0.25
	P^{min}	190	41	2.17	1400	0.25	0
	P^{max}	230	50	2.65	1750	3	0.50

The heat transfer coefficient due to losses from the tank to ambient surrounding air was assessed to be 2.6WK^{-1} taking into account the factory-applied insulation and overall tank surface area.

3.4. Results

Results of the parameter fitting for both PCM samples based on the first pair of experiments are given in Table 2 separated into charge phase and discharge phase results. For convenience, the water/PCM AU values have been expressed here in the units Wm^{-2}K^{-1} by taking into account the overall heat surface area of the internal coils of the test tank (3.8m^2). Though there is broad consistency in the PCM properties between the charge and discharge test phases, it is notable that the AU values during the charge phase are much higher than during discharge. This is to be expected since, though the thermal conductivity of the liquid and solid phases of samples used in this work are not known, it is generally the case that the conductivity is higher in the solid phase than in the liquid phase [4]. Therefore, heat transfer to PCM in its solid state will be higher than in its molten state. This finding is consistent with other results in the literature [11,12].

Table 2
Results of fitted model parameters

Sample/test	Fitting RMSE (K)	h_{pcm-F} (kJkg^{-1})	T_{pcm-F} (°C)	$\bar{c}_{pcm}$ (kJkg^{-1}K^{-1})	ρ_{pcm} (kgm^{-3})	F (-)	AU_{wp} (Wm^{-2}K^{-1})
S32 ch.	0.21	199.9	32.14	1.96	1460	0.55	120.8
S32 disch.	0.16	200.0	31.49	2.00	1460	0.87	45.0
S46 ch.	0.22	210.0	45.99	2.41	1587	0.94	197.1
S46 disch.	0.14	209.9	44.01	2.32	1587	0.86	51.1

Using these fitted values, the model described in sections 3.1-3.2 was used to predict tank water outlet temperatures against time based on the second set of experimental results (i.e. the results allocated for fitted model testing). Results are plotted in Fig. 5(a) – Fig. 5(d). In summary, the root-mean-square errors between predicted and measured tank water outlet temperatures were found to be 0.25K (charge phase), 0.18K (discharge phase) for the S32 sample, and 0.22K

(charge phase), 0.29K (discharge phase) for the S46 sample. These results are well within the temperature measurement uncertainty of ±0.5K.
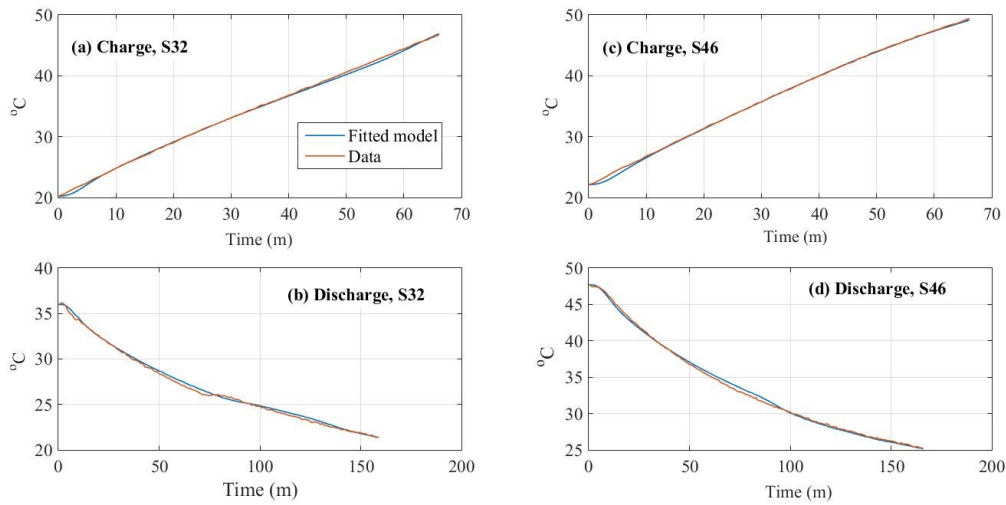
Fig. 5. Fitted hybrid tank model: predicted and measured outlet water temperature
(a) Charge phase, S32; (b) Discharge phase, S32; (c) Charge phase S46; (d) Discharge phase, S46

4. System Simulation with a Proposed Thermal Store Design

In order to explore the potential of a hybrid water/PCM thermal storage tank using coil-encapsulated PCM in a domestic grid-stress application, results from Section 3.4 were scaled up to a tank size that might be fitted into a household kitchen space. This was then coupled with other component models to form a fully dynamic thermal system simulation as a vehicle for such an analysis.

Modern domestic kitchens tend to be designed around a modular planning dimension of 300mm. An under-bench cupboard unit will usually occupy a plan space of 600mm × 600mm with a typical bench height of 900mm. A thermal storage tank occupying such a space would have an outer diameter of 510mm and height 790mm which would then leave an adequate margin for the application of thermal insulation to the outside of the tank as well as a bench material over it. A set of 8 concentric PCM coils with outer pitch diameters ranging from 163mm to 490mm could be accommodated in this tank. (The diameters of the test coils, at 340mm and 410mm are, approximately, at the median and upper quartile boundary of this range.) With the height available, and assuming 23.4mm (outer diameter) thin-wall stainless steel tube, up to 19 coil turns could be achieved for each coil. Scaling this up, a nominal hybrid thermal storage tank fitting into one standard kitchen under-bench space would have a total PCM inventory of 67.1 litres and a surrounding water space of 92.2 litres, giving an overall tank capacity of just under 160 litres. (For increased thermal storage, several such modules could be coupled together.)

4.1 Simulation Model Development

A fully dynamic simulation model consisting of a house equipped with a conventional low-grade hot water heating system (hot water radiators), domestic hot water generation and an air-source heat pump coupled to the hybrid thermal store. The domestic hot water generation method consisted of primary heating (from the heat pump/hybrid store), a direct-electric boost heater, a direct-electric pasteurising heater and a small buffer water store of 25L capacity. With

a pasteurising heating cycle, the nominal DHW buffer store temperature can be maintained at a value compatible with the normal heat pump operation.

Two types of coupled thermal store were explored – the scaled-up hybrid thermal store as described above and an alternative water thermal store (of the same overall volume as the hybrid store) as a comparison. In this illustration, only the S46 PCM sample was considered in the store specification. The model has been developed using Matlab/Simulink. Details of the model including all variable flow paths are shown in Fig. 6 and details of the individual model components can be found in the Appendix.
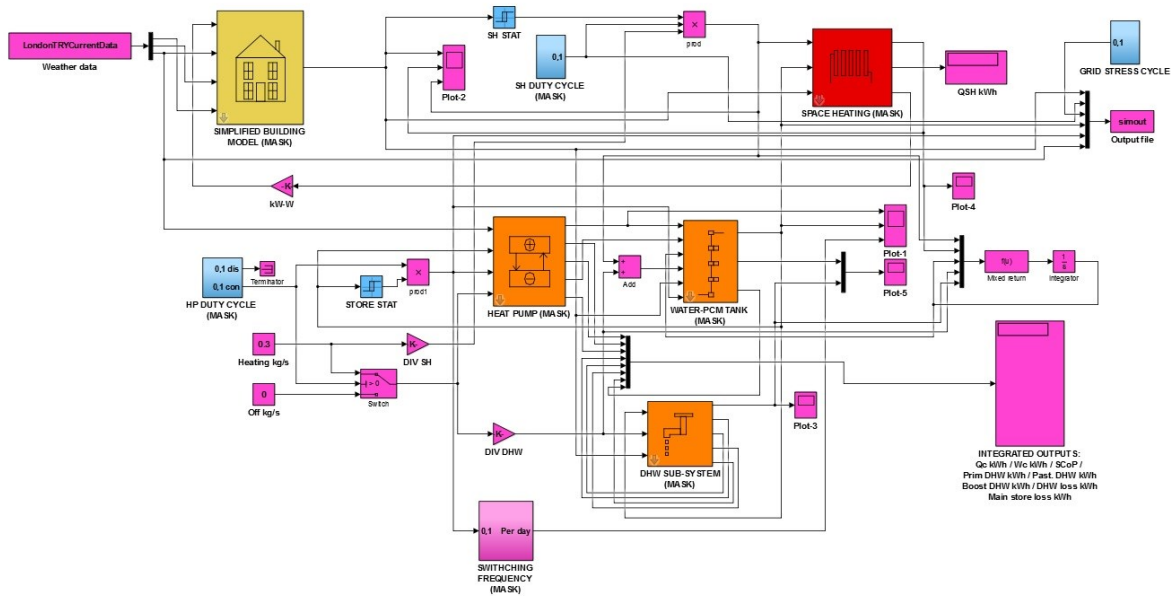
Fig. 6. Matlab/Simulink model of the domestic heating system with hybrid thermal store

The house type included in the model consists of a 'modern' end-terrace/semi-detached house with a gross floor area of 100m^2 constructed to the standards set out in the current edition of the United Kingdom Building Regulations, Part L [23]. The house has been located in London and the current (reference) test reference year for London from the CIBSE's future weather data series was used [24].

4.2 Results from a 'Clean Cycle' Simulation

In order to gain an insight into the behaviour of the thermal store free from the interaction of other 'balance of system' plant and controls, an initial simulation was conducted based on the heat pump and store only (all other variable connections were disabled). This so-called 'clean simulation' was excited with a switch-on step change to the heat pump (i.e. store charging) followed after the completion of charging with a switch-off step change. The heating thermostat, positioned on the tank discharge and acting directly on the heat pump has a set point (upper limit) of 50ºC and a switching dead-band of 5K. Results generated using both the hybrid store and water store are shown in Fig. 7.

Some features in these results are noteworthy:

- Because the heat pump is switched according to its inlet water temperature, its outlet water temperature will be a little higher which results in a small amount of overshoot in the tank outlet temperature most evident in the water tank charge transient.
- No such overshoot is initially evident for the hybrid tank because, as the heat pump first switches off, heat is still being accumulated in the PCM but gradually this temperature increases towards to same degree of overshoot as the PCM becomes full melted.
- At the sixth thermostat switch-off instant, the PCM is now fully melted and charging is complete. This has taken just over 3h for the hybrid tank and just over 1h for the water tank, from an initial cold start.
- The slight downward gradient (most evident in the water tank charge transient) is due to tank heat loss to ambient surroundings.
- During discharge, the impact of the PCM can be clearly seen. It sustains the design space heat load of the house (4.7kW) for a full 2h before declining over the subsequent 2h. For most milder days, this would give independent heating system operation throughout most of the grid-stress period. The water tank can supply only about half of the design rated load on average over a 2h period only.
- The heating spike evident for a very short period as soon as heat discharge starts is due to the short-lived wide heating water temperature differential as warm water from the heating system displaces cold room-temperature water from the radiators. This is quite normal during the cold start-up of a heating system.
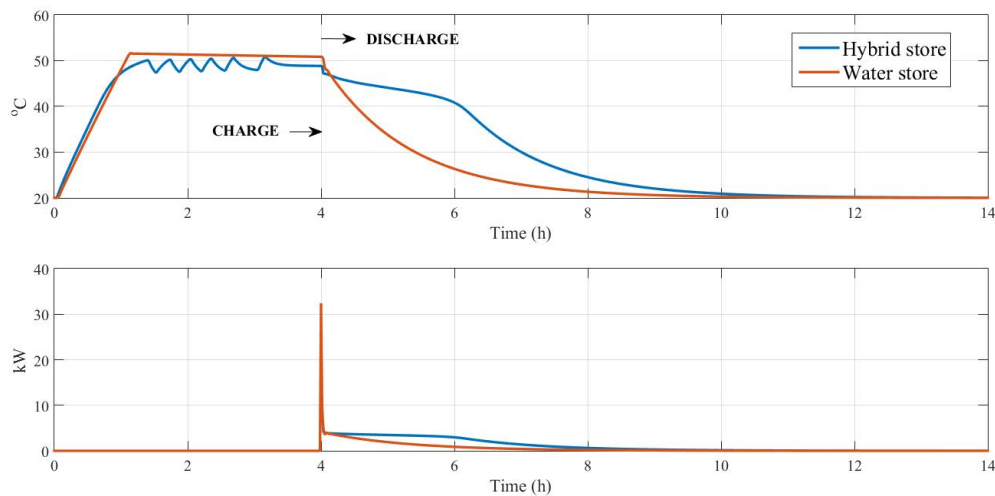
Fig. 7. Simulation of a simplified charge and discharge cycle

4.3 Results from a Full Seasonal System Simulation

A full seasonal system simulation was carried out based on both the hybrid thermal storage tank and the water tank. The heat pump operating schedule was set so that heat pump is offered to the thermal store at all times other than the grid-stress period (16:00h – 20:00h during winter week days) at which times the heat pump is switched off though other system components operate as normal. Space heating is offered during daytime periods in winter only – further details can be found in the Appendix. In all cases, space heat and domestic hot water heat are taken from the thermal store.

The space heating is controlled to a mean house temperature set point of 20°C with a thermostat dead-band of ±1K. The domestic hot water (DHW) includes a direct-electric top-up heater to

ensure a secondary tap water temperature of 45°C together with a direct-electric pasteurising heater in the DHW buffer tank with a set point of 70°C and a switching frequency of once per week.

Annual simulations were carried out for an arbitrary range of overall storage tank capacities: the nominal value of 159L as described in Section 4; half of this value (79.5L); one quarter of this value (40L) and twice the nominal capacity (318L). Parameters of the nominal hybrid store as detailed in the Appendix were simply scaled in proportion to the capacity value. For comparison, the same volume capacities of a simple water tank thermal store were also included.

Results of the simulations are summarised in Table 3 (energy and performance) and Fig. 8 (comfort). Comfort results are expressed as the percentages of the total grid stress period time (688h per year) during which mean house temperature is less than the temperature indicated along the horizontal axis of the graph – referred to here as grid-stress period comfort violations. Because the simulations used a nominal heating set point of 20°C with a switching dead-band of ±1K, comfort violations below 19°C are considered to be most serious.

a) Energy and performance

In Table 3, the seasonal coefficient of performance, *SCoP*, for the heat pump is the total heating delivered by the heat pump over the annual cycle divided by the corresponding electricity used by the heat pump. The total heating delivered is that due to space heating, DHW primary heating and a share of the tank losses (a share because some of the tank loss will be accounted for in the direct-electric boost heating and pasteurisation heating loads). The total electricity values consist of the heat pump electricity plus direct electricity due to DHW boost and pasteurisation loads. The simulated seasonal performance factor, *SPF*, is the total heating delivered including DHW boost and pasteurisation loads, divided by the total electricity used and the adjusted *SPF* is the same with the exception that the buffer and main store tank losses are excluded in the total heat delivered figure. (The heating circulating pump electricity has been neglected in all annual energy loads.)

Table 3
Annual energy and performance results of simulations

Annual Result	Hybrid Storage Tank				Water Tank			
	40L	79.5L	159L	318L	40L	79.5L	159L	318L
Thermal loads (kWh):								
Space heating	2999	3129	3242	3261	2958	3035	3124	3220
DHW primary	1625	1684	1584	1492	1755	1737	1625	1523
DHW boost	501	447	464	506	462	458	500	523
DHW pasteurising	116	141	223	251	81.1	118	181	252
Main store losses	79.1	132	212	334	171	268	424	680
DHW buffer losses	81.4	84.9	83.8	82.2	86.7	84.7	83.4	82.9
Total electricity (kWh)	2162	2294	2468	2483	2063	2132	2266	2447
Performance:								
Heat pump *SCoP*	3.04	2.90	2.83	2.95	3.21	3.24	3.26	3.25
Heat pump *SPF*	2.46	2.41	2.32	2.36	2.63	2.63	2.58	2.54
Heat pump adjusted *SPF*	2.38	2.32	2.20	2.19	2.50	2.47	2.36	2.22
Heat pump max starts/day	8	6	4	2	8	6	4	3

The annual thermal load met by the heat pump is higher for the water storage tank options than for the hybrid store options. Practically all of this is accounted for by the main store standing loss which is approximately twice as high for the water store as for the hybrid store options. The reason for this is that the mean storage temperature of the water tank options is higher than for the hybrid tank options due to higher responsiveness (i.e. see Fig. 7).

With the exception of the smallest tank size, boost DHW heating is higher for the water tank than for the hybrid tank. The reverse of this is the case for pasteurising water heating (except for the largest tank size where they are practically the same). The reason for the first of these anomalies is that the DHW buffer tank can call on more heat from the hybrid store before the heat pump needs to re-start (or the boost heater activate) than is the case with the water tank main store and this is especially the case with 'spikey' hot water demand loads. The reason for the second anomaly (pasteurising heat) is, again, due to the average water temperature in the main water tank being higher than in the hybrid tank option and this in turn increases the water temperature in the DHW buffer tank with the result that the pasteurising cycle temperature rise is slightly lower for the water tank case than the hybrid store case.

This combination of conditions means that the hybrid store cases draw slightly more total electricity that the water store cases but the latter needs to deliver more heat mainly due to higher main store tank losses. Thus the *SCoP* values are slightly higher for the water tank cases whereas the adjusted *SPF* values are in closer alignment.

In terms of energy and performance however, it can be concluded that both sets of main thermal storage options show broadly similar behaviour. As will be seen below, it is comfort through the crucial grid-stress afternoon/evening period where an advantage in the greater thermal storage density of the hybrid store begins to open up.

b) Comfort

Percentages of the overall annual grid-stress period for which mean house internal temperatures are below certain values are presented in Fig. 8. For the smallest tank capacity, the impact of the PCM contribution is low which means that the hybrid tank of this capacity offers no advantage over a water tank of the same size (i.e. both behave poorly). At the other end of the scale, a large tank offers high thermal storage in relation to demand whether using only water or a combination of storage media and so, again, there is little advantage in hybridisation. Where an advantage opens up is in the intermediate tank size suggested in Section 4 with an overall capacity of 159L (of which 42% is salt-hydrate PCM). Fig. 8 shows that a water tank of this capacity would lead to average house temperatures dropping below 18°C for 10% of the early evening grid-stress period but reducing to just 1.6% of this period when using the hybrid storage option. At a tighter threshold of 19°C, lower mean house temperatures would be experienced for 22.7% of the grid-stress period when using a water store whereas this would be just 5.8% when using a hybrid store of the same overall volume.
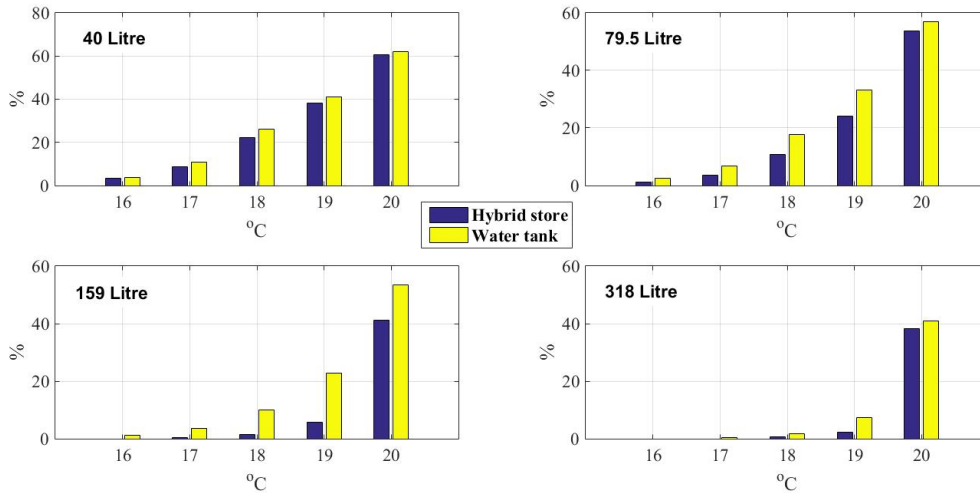
Fig. 8. Grid-stress period comfort violations under various storage capacities

5. Conclusions

Thermal storage for use with domestic heat pumps has been explored in this paper. The focus has been on developing a compact thermal store design that can help to maintain comfort during the period of highest electrical grid demand (the so-called grid-stress period) when, ideally, the heat pump should not be operational. The work is predicated on expected high growth in the use of heat pumps for domestic heating in the future.

A novel hybrid store design has been considered consisting of a salt-hydrate phase change material encapsulated in helical coils inserted into an otherwise conventional water tank. Experiments were carried on a conventional water tank in which its internal coils were alternately charged with different samples of phase change material. A model-based approach was used to extract heat transfer parameters related to the water space and phase change material space in the storage tank. Heat transfer coefficients ranging from $45 \mathrm{Wm}^{-2}\mathrm{K}^{-1}$ (during store discharge) to just under $200 \mathrm{Wm}^{-2}\mathrm{K}^{-1}$ (during charging) were obtained. A new method for describing the relationship between phase change material temperature and enthalpy during melting and freezing has been proposed.

Illustrative simulations were carried out on a suggested compact store design which could be accommodated within a standard domestic kitchen under-bench cupboard space coupled to an air-source heat pump to meet both space heating and domestic water heating demands. Broadly similar seasonal energy and performance results were obtained from the simulation when comparing the hybrid compact store with a simple water tank store of the same overall capacity. However the hybrid thermal store was found to sustain better comfort conditions throughout the grid-stress period than could be achieved when using a water tank of the same capacity. Average house temperature were predicted to fall below $19^{\circ}\mathrm{C}$ for 22.7% of the grid-stress period when using a water tank thermal store whereas this dropped to just 5.8% when using the hybrid store of the same volume.

Many avenues of further work present themselves from what has been done here:

- Further experiments using PCM in coils with alternative pitch diameters and tube diameters to determine the influence of coil geometry.

- Development and field-testing of a prototypical hybrid store.
- Introduction of an optimisation algorithm to the simulation model to assist in hybrid store design and control scheduling.
- Investigations into corrosion, practical coil lifespan and replacement logistics.
- Extended modelling to include alternative control strategies including variable speed heat pump drives with modulating control.
- Economic studies into extended duty cycles including off-peak heating and peak-lopping strategies.
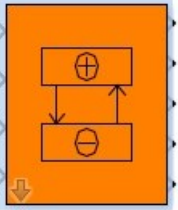
References

[1]   DECC, The future of heating: meeting the challenge. Available online: https://www.gov.uk/government/uploads/system/uploads/attachment_data/file/190149/16_04-DECC-The_Future_of_Heating_Accessible-10.pdf (accessed 21 07 17).

[2]   National Grid Data Explorer. UK electricity demand data 2011-2016. Available online: http://www2.nationalgrid.com/uk/Industry-information/Electricity-transmission-operational-data/Data-Explorer/ (accessed 19 07 17).

[3]   B. Zalba, J.M. Marin, L.F. Cabeza, H. Mehling, Review on thermal energy storage with phase change: Materials, heat transfer analysis and applications, Applied Thermal Engineering 23 (2003) 251-283.

[4]   F. Agyenim, N. Hewitt, P. Eames, M. Smith, A review of materials, heat transfer and phase change problem formulation for latent heat thermal energy storage systems (LHTESS), Renewable and Sustainable Energy Reviews 14 (2010) 615-628.

[5]   J.P. da Cunha, P. Eames, Thermal energy storage for low and medium temperature applications using phase change materials – A review, Applied Energy 177 (2016) 227-238.

[6]   M.K. Anuar Sharif, A.A. Al-Abidi, S. Mat, K. Sopian, M.H. Ruslan, M.Y. Sulaiman, M.A.M. Rosli, Review of the application of phase change material for heating and domestic hot water systems, Renewable and Sustainable Energy Reviews 42 (2015) 557-568.

[7]   D.N. Nkwetta, F. Haghighat, Thermal energy storage with phase change material – A state-of-the-art review, Sustainable Cities and Society 10 (2014) 87-100.

[8]   P. Moreno, C. Solé, A. Castell, L.F. Cabeza, The use of phase change materials in domestic heat pump and air-conditioning systems for short term storage: A review, Renewable and Sustainable Energy Reviews 39 (2014) 1-13.
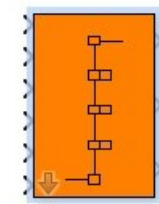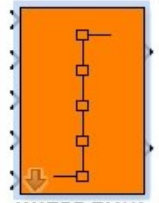
[9]   A.A. Pardiñas, M.J. Alonso, R. Diz, K.H. Kvalsvik, J. Fenrández-Seara, State-of-the-art for the use of phase change materials in tanks coupled with heat pumps, Energy and Buildings 140 (2017) 28-41.

[10]   M. Rastogi, A. Chauhan, R. Vaish, A. Kishan, Selection and performance assessment of phase change materials for heating, ventilation and air-conditioning, Energy Conversion and Management 89 (2015) 260-269.

[11]   J.C. Choi, S.D. Kim, Heat transfer in a latent heat-storage system using $MgCl_2$-$6H_2O$ at the melting point, Energy 20 (1995) 13-25.

[12]   F. Agyenim, N. Hewitt, The development of a finned phase change material (PCM) storage system to take advantage of off-peak electricity tariff for improvement in cost of heat pump operation, Energy and Buildings 42 (2010) 1552-1560.

[13]   A. Frazzica, M. Manzan, A. Sapienza, A. Freni, G. Toniato, G. Restuccia, Experimental testing of a hybrid sensible-latent heat storage system for domestic hot water applications, Applied Energy 183 (2016) 1157-1167.

[14]   R.E. Murray, D. Groulx, Experimental study of the phase change and energy characteristics inside a cylindrical latent heat energy storage system: Part 1 consecutive charging and discharging, Renewable Energy 62 (2014) 571-581.

[15]   J. Porteiro, J.L. Míguez, B. Crespo, L.M.L. González, J. De Lara, Experimental investigation of the thermal response of a thermal storage tank partially filled with different PCMs (phase change materials) to a steep demand, Energy 91 (2015) 202-214.

[16]   C. Zauner, F. Hengstberger, B. Mörzinger, R. Hofmann, H. Walter, Experimental characterisation and simulation of a hybrid sensible-latent heat storage, Applied Energy 189 (2017) 506-519.

[17]   N.J. Kelly, P.G Tuohy, A.D. Hawkes, Performance assessment of tariff-based air source heat pump load shifting in a UK detached dwelling featuring phase change-enhanced buffering, Applied Thermal Engineering 71 (2014) 809-820.

[18]   Za. Khan, Zu. Khan, K. Tabeshf, Parametric investigations to enhance thermal performance of paraffin through a novel geometrical configuration of shell and tube latent thermal storage system, Energy Conversion and Management 127 (2016) 355-365.

[19]   A. Campos-Celador, G. Diarce, J.T. Zubiaga, T.V. Bandos, A.M. Garcia-Romero, L.M. Lopéz, J.M. Sala, Design of a finned plate latent heat thermal energy storage system for domestic applications, Energy Procedia 48 (2014) 300-308.

[20]   A. Najafian, F. Haghighat, A. Moreau, Integration of PCM in domestic hot water tanks: Optimization for shifting peak demand, Energy and Buildings 106 (2015) 59-64.

[21]   M. Nabavitabatabayi, F. Haghighat, A. Moreau, P. Sra, Numerical analysis of a thermally enhanced domestic hot water tank, Applied Energy 129 (2014) 253-260.

[22]   S. Pincemin, R. Olives, X. Py, M. Christ, Highly conductive composites made of phase change materials and graphite for thermal storage, Solar Energy Materials and Solar Cells 92 (2008) 603-613.

[23]   The Building Regulations 2010. Conservation of Fuel and Power in New Dwellings – Approved Document L1A [Online]. Available at: https://www.gov.uk/government/publications/conservation-of-fuel-and-power-approved-document-l (accessed 19 07 17).

[24]   CIBSE TM48. Use of climate change scenarios for building simulation: The CIBSE future weather years, 2009. London: Chartered Institution of Building Services Engineers.

[25]   PCM Products Ltd, PlusICE Phase Change Materials [Online]. Available at: http://www.pcmproducts.net/files/PlusICE%20Range-2013.pdf (accessed 04 07 17).

[26]   C.P. Underwood, An improved lumped parameter method for building thermal modelling, Energy and Buildings 79 (2014) 191-201.

[27]   J. Fong, J. Edge, C.P. Underwood, A. Tindale, S.E. Potter, Performance of a dynamic distributed element heat emitter model embedded into a third-order lumped parameter building model, Applied Thermal Engineering 80 (2015) 279-287.

[28]   C.P. Underwood, M. Royapoor, B. Sturm, Parametric modelling of domestic air-source heat pumps, Energy and Buildings 139 (2017) 578-589.

[29]   BS EN 13203-2:2015 Gas-fired domestic appliances producing hot water. Part 2: Assessment of energy consumption. BSI Standards Publication.
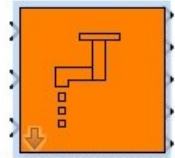
Block type (Fig. 5) & modelling method	Inputs (symbols list)	Outputs (symbols list)	Parameters (symbols list)	Parameter values used
SIMPLIFIED BUILDING MODEL (MASK) Details of the main approach used in the construction of this model can be found in [26].	T_{ai} (ºC)	Q_h (W) T_{ao} (ºC) $I_{g,hor}$ (Whm⁻²) N_{day} (-)	V (m³) ACR_i (h⁻¹) ACR_v (h⁻¹) Q_{cas} (W) τ (-) FR_{Qcas} (-) FR_h (-) ϕ (degrees) Each window: A (m²) U (Wm⁻²K⁻¹) β (degrees) α (degrees) Each element: A (m²) R (m²KW⁻¹) C (Jm⁻²K⁻¹) f_i (-) f_o (-) g_i (-)	280 0.5 2.5 500 0.6 0.6 0.7 52 3 windows: 11.5,2,11.5 3,3,3 90,90,90 180,90,0 4 elements: 94,50,50,130 6.7,2.2,7.9,2 222,961,60,25 0.012-0.044 0.008-0.06 0.176-0.5
SPACE HEATING (MASK) Modelling method details in [27].	m_h (kgs⁻¹) T_{wi} (ºC) T_{ai} (ºC)	T_{wo} (ºC) E_h (kWh) Q_h (kW)	$Q_{h,des}$ (W) $\Delta T_{h,ai,des}$ (K) C_h (JK⁻¹)	4700 25 2×10^6
HEAT PUMP (MASK) Modelling method details in [28].	T_{ao} (ºC) T_{wi} (ºC) S_{hp} (-) m_w (kgs⁻¹)	T_{wo} (ºC) E_W (kWh) E_h (kWh) m_w (kgs⁻¹) $SCoP$ (-)	Source fluid Refrigerant θ_{hp} (s) V_d (m³s⁻¹) W_{aux} (W) $\Delta T_{pinch,ev}$ (K) $\Delta T_{pinch,co}$ (K)	Air R410A 60 1.5×10^{-3} 200 5 5

Block type (Fig. 5) & modelling method	Inputs (symbols list)	Outputs (symbols list)	Parameters (symbols list)	Parameter values used
WATER-PCM TANK (MASK) Details of the modelling method are in Section 3.1. In this work, the model was interpreted as a 10-zone model.	$T_{wi,pri}$ (°C)	T_{wo} (°C)	V_{pcm} (m³)	0.067 (nom.)
	$m_{w,pri}$ (kgs⁻¹)	$T_{pcm,n}$ (K)	V_{wi} (m³)	0.002 (nom.)
	$T_{wi,sec}$ (°C)	E_{al} (kWh)	V_{wo} (m³)	0.005 (nom.)
	$m_{w,sec}$ (kgs⁻¹)		V_{wp} (m³)	0.085 (nom.)
	T_{ai} (°C)		ρ_{pcm} (kgm⁻³)	1587
	S_{hp} (-)		c_{pcm} (kJkg⁻¹K⁻¹)	2.367
			h_{pcm-F} (kJkg⁻¹)	209.95
			T_{pcm-F} (°C)	45
			$AU_{wp,ch}$ (kWK⁻¹)	2.580
			$AU_{wp,dis}$ (kWK⁻¹)	0.688
			F (-)	0.903
			K_{al} (WL⁻¹K⁻¹)	0.01
			T_{wp0} (°C)	20
WATER TANK Alternative 'control case' water tank model, zoned as above.	$T_{wi,pri}$ (°C)	T_{wo} (°C)	V_w (m³)	0.159 (nom.)
	$m_{w,pri}$ (kgs⁻¹)	E_{al} (kWh)	K_{al} (WL⁻¹K⁻¹)	0.01
	$T_{wi,sec}$ (°C)		T_{w0} (°C)	20
	$m_{w,sec}$ (kgs⁻¹)			
	T_{ai} (°C)			

Block type (Fig. 5) & modelling method	Inputs (symbols list)	Outputs (symbols list)	Parameters (symbols list)	Parameter values used
DHW SUB-SYSTEM (MASK) DHW demand is fixed using one of the standard 'tapping cycles' given in [29]. The 'medium' demand pattern is consistent with a small family.	$T_{wi,pri}$ (ºC)	$T_{wo,pri}$ (ºC)	Demand type: (L, M, H, VH)	M (medium)
	$m_{w,pri}$ (kgs^{-1})	E_{pri} (kWh)	V_w (m^3)	0.025
	T_{ai} (ºC)	E_{past} (kWh)	T_{w0} (ºC)	20
		E_{boost} (kWh)	T_{cwf} (ºC)	15
		E_{al} (kWh)	$T_{dhw,boost}$ (ºC)	45
			Q_{past} (kW)	3
			$T_{w,past}$ (ºC)	70
			K_{al} (WL^{-1}K^{-1})	0.01
			V_{buffer} (litre)	25
			Demand type	'Medium'

Block (Fig. 5)	Role/Description
Weather data	Reads weather data from a London Test Reference Year [24]
SH STAT	Space heating thermostat. Switch on at $T_{ai} \leq 19$ºC, off 21ºC.
STORE STAT	Heat pump/store thermostat. Switch on at $T_{wo} \leq 40$ºC, off 50ºC.
HP DUTY CYCLE	Heat pump availability switch. Always available except 16:00-20:00 daily.
SH DUTY CYCLE	Space heating availability switch. 06:00-08:00h and 16:00h-23:00h winter weekdays; 08:00-12:00h and 16:00h-23:00h winter weekend days. Off at all other times and continuously off May – August.
GRID STRESS CYCLE	16:00h – 20:00h each winter weekday (i.e. January – April and September – December).
SWITCHING FREQ.	Tracks the plant switching instants due to the combined gating of the availability switch and heating thermostat and calculates the total number of switching events for each day.